



Effect of initial damage on remotely triggered rockburst in granite: an experimental study

Jianqing Jiang^{1,2} · Guoshao Su¹ · Xiaohe Zhang¹ · Xia-Ting Feng²

Received: 13 October 2019 / Accepted: 17 February 2020 / Published online: 5 March 2020
© Springer-Verlag GmbH Germany, part of Springer Nature 2020

Abstract

A remotely triggered rockburst is a typical engineering geology disaster that occurs during the excavation of hard rock at depth. Damage in the rock mass naturally exists and will also be induced by the construction of underground excavation. These damages, in turn, influence the occurrence and intensity of a rockburst. However, this problem, which draws significant public attention, remains unsolved. In the present study, the effect of the initial damage on a triggered rockburst of granite is investigated. Rectangular prismatic rock specimens with different initial damage D (0, 0.2, 0.3, 0.4, 0.6, and 0.7) are prepared by using heat-treatment (25, 200, 300, 400, 500, and 600, respectively). The initial damage is determined by the ratio of the P wave velocity of the specimen heat-treated at a specific temperature to that without heat-treatment. Then, remotely triggered rockburst simulations are conducted on the specimens with coupled static-dynamic loads exerted using an improved true-triaxial testing machine. The failure mode, deformation characteristics, fracture features, and kinetic energy of the ejected fragment of the tested specimen are systematically investigated. The experimental results indicate that for a given initial damage, a threshold of static stress exists, and beyond this threshold, a dynamic disturbance can trigger a rockburst. Additionally, it is found that a dynamic disturbance can much more easily induce a triggered rockburst as the level of initial damage increases. However, the kinetic energy of ejected fragments increases to a peak and then decreases as the initial damage increases. The maximum kinetic energy appears at an initial damage $D = 0.3$. Therefore, another interesting finding is a specific initial damage can induce the most violent triggered rockburst.

Keywords Rockburst · Triggered rockburst · Initial damage · Dynamic disturbance · True-triaxial test

Introduction

Rockburst is a violent dynamic rock failure that is frequently encountered during underground excavation (Fan et al. 2016; He et al. 2015; Huang et al. 2018; Su et al. 2017c; Xu et al. 2016; Zhao and Cai 2014). As characterized by the ejection of rock fragments, this rock failure is a destructive engineering geological disaster that can kill workers, destroy equipment, and damage mining and tunnel construction (Akdag et al.

2018; Cai 2013; Chen et al. 2014; Fakhimi et al. 2016; Li et al. 2012; Zhang et al. 2012). With underground excavation migrating deep underground, rockburst becomes an increasingly important issue in the fields of mining, tunneling, and underground excavations. Considerable research efforts have been devoted to investigating rockbursts, and many studies exist in terms of mechanism revelation (Feng et al. 2015; Huang et al. 2018; Manouchehrian and Cai 2018; Qiu et al. 2014; Sun et al. 2017; Zhou et al. 2015), occurrence process description (Feng et al. 2017; Feng et al. 2016; Gong et al. 2019a; He et al. 2015; Hu et al. 2019; Jiang et al. 2010; Li et al. 2012; Zhu et al. 2010), classification (Gong et al. 2019c; He et al. 2012; Hedley 1992; Kaiser 1996; Ortlepp and Stacey 1994), prediction (Gong et al. 2019b; Pu et al. 2019; Xu et al. 2016), and prevention (Cai 2013; Kaiser and Cai 2012; Simser et al. 2002). However, the current recognition technique is not sufficient to prevent a rockburst entirely, because, most importantly, a rockburst is an extremely complicated phenomenon influenced by many factors. Additional studies including field

✉ Guoshao Su
guoshaosu@gxu.edu.cn

¹ Key Laboratory of Disaster Prevention and Structural Safety of Ministry of Education, School of Civil Engineering and Architecture, Guangxi University, Nanning 530004, China

² Key Laboratory of Ministry of Education on Safe Mining of Deep Metal Mines, Northeastern University, Shenyang 110819, China

investigations, laboratory experiments, and numerical simulations on rockbursts are urgently needed.

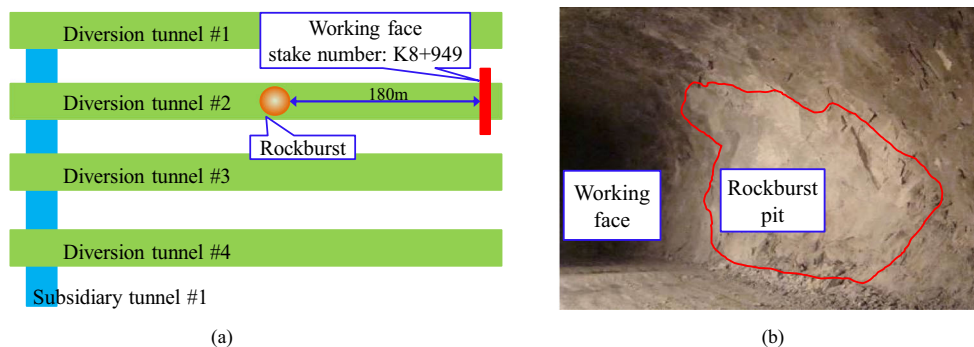
According to the triggering mechanism, rockbursts can be generally classified as either self-initiated rockbursts or triggered rockbursts (Kaiser 1996). A self-initiated rockburst is always encountered in the surrounding rocks near the excavated boundary and caused by the gradual increase of the tangential stress due to the stress redistribution (concentration) after excavation. A triggered rockburst occurs in a highly stressed rock masses disturbed by dynamic loading including blasting and drilling, an adjacent rockburst, or seismic activity (Huang and Wang 1999; Zhu et al. 2010). A remotely triggered rockburst usually lags the excavation in terms of time and space. For instance, as shown in Fig. 1, during the construction of the #2 diversion tunnel of the Jinping II Hydropower Station, a triggered rockburst, which was approximately 180 m away from the tunnel face, was induced by remote blasting at the tunnel face (Feng et al. 2013). Unfortunately, a remotely triggered rockburst cannot be accurately predicted, and forecasting the timing of the occurrence is still especially difficult. Due to its dangerous and unpredictable nature, remotely triggered rockbursts seriously threaten engineers and construction equipment during underground excavation. Therefore, a good understanding of remotely triggered rockbursts is vital to the design and construction of the excavation of hard rock at depth. Existing studies provide meaningful insight into the characteristics and mechanism of self-initiated rockbursts based on indoor rock mechanics tests, while experimental investigations into remotely triggered rockbursts are still limited.

In the past few years, significant progress has been made in characterizing rockbursts. As early as the 1960s, the uniaxial compressive test was performed to study the energy characteristics of rock masses subjected to rockbursts (Cook 1963; Fakhimi et al. 2016; Jiang et al. 2015; Nemat-Nasser and Horii 1982; Qiu et al. 2014; Wang and Park 2001). Subsequently, biaxial (Zhang et al. 2017) and conventional triaxial tests (Cho et al. 2005; Höfer and Thoma 1968; Hua and You 2001; Huang et al. 2001) were conducted to describe a rockburst. In recent years, a testing method, called the one-free face true-

triaxial rockburst test, has been developed and widely used to study the rockburst ejection process, which significantly promotes the investigation of the rockburst mechanism (He et al. 2010; He et al. 2007; Su et al. 2017c; Su et al. 2017d; Zhao and Cai 2014; Zhao et al. 2014). The focus of the tests mentioned above is the self-initiated rockburst caused by static stress without dynamic load. However, in rock engineering practice, rocks are always subjected to a hybrid static and dynamic loading and behave differently compared with solely static or dynamic stresses (Wu et al. 2016). Dynamic loading is sometimes a controlling factor that can trigger or induce rock failure during underground excavation, especially for high-initial geo-stressed conditions. Thus, it is desirable to understand a triggered rockburst that occurs in statically stressed rocks subjected to a dynamic disturbance. However, existing studies related to triggered rockbursts primarily focus on the influence of the geo-stress condition, especially the contribution of the dynamic disturbance, on the triggered rockburst characteristics (He et al. 2012; Su et al. 2017b; Su et al. 2018; Zhu et al. 2010). In addition to the geo-stress condition, the rock lithology (Li et al. 2015) and anisotropy (Dai and Xia 2010; Manouchehrian and Cai 2017; Xia et al. 2008) also affect the rock failure during underground excavation. Hence, further study should be implemented to characterize a triggered rockburst and its influencing factors. In the present study, an investigation of the influence of initial damage on a remotely triggered rockburst, which is seldom involved, is conducted.

Generally, all rock masses, including natural rock masses and engineering rock masses, have varying degrees of damage. Rock damage is the degradation of the macromechanical properties caused by initiation, propagation, and coalescence of microdefects. For rock masses in which an underground excavation is constructed, the rock damages are induced by changes in the stress state and boundary condition. Before excavation, the burial history, such as tectonic loading, has already resulted in rock damage in the form of existing microdefects. In addition, under a high-ground stress condition, loosening blasting, and pressure relief holes, which are usually applied to a stressed rock mass to partially release the

Fig. 1 Rockburst triggered by blasting at a remote tunnel face during the excavation of the diversion tunnels of the Jinping II Hydropower Station (Feng et al. 2013). **a** Position of the triggered rockburst, **b** Photo of the triggered rockburst



stress, also result in rock damage (Feng et al. 2013). During excavation, creating an opening continually degrades the rock masses. After excavation, the increasing tangential stress and applied dynamic disturbance inevitably cause further damage to form in the rock masses. Previous studies indicate that rock damage significantly affects the mechanical behavior of rocks (Board and Fairhurst 1983; Brady and Brown 2013). For instance, rocks with more damage can be more easily crushed (Doan and D'Hour 2012), and damage decreases the strength and elastic modulus of a stressed rock (Mao et al. 2015; Peng et al. 2016a). For underground engineering projects, we primarily focus on rock mechanical behavior after excavation. Therefore, the rock damage that formed before and during excavation, which is called initial damage in this paper, should be fully considered. Initial damage will affect the triggered rockburst caused by a subsequent stress concentration or dynamic disturbance after excavation. Hence, gaining a good understanding of the triggered rockburst occurring in the damaged rock mass is significant for underground excavation. However, the materials used for rockburst investigations in existing studies are usually intact rocks. An experimental study on rockbursts in a damaged rock has not been systematically conducted.

In the present study, granite specimens heat-treated at temperatures of 200 °C, 300 °C, 400 °C, 500 °C, and 600 °C were used to investigate the effect of initial damage on remotely triggered rockburst. A true-triaxial rockburst testing machine was used to apply coupled static and dynamic stresses on prismatic rectangular specimens to simulate remotely triggered rockburst. In the following sections, the detailed preparation process of the specimen, the true-triaxial rockburst testing machine used, and the loading path are introduced. Subsequently, the testing results are presented. Meanwhile, the rockburst process, failure form, fragments, and kinetic energy of the ejected fragments under different initial damage conditions were systematically analyzed. Finally, the main conclusions are drawn.

Specimen preparation and testing methodology

Specimen preparation

The used rock material is coarse-grained granite obtained from Cenxi in the southeast region of Guangxi Zhuang Autonomous Region, China. To obtain the desired specimens, rock blocks with dimensions of 101 mm × 101 mm × 201 mm were cut from a large rock block. Then, these rock blocks were sliced into specimens with dimensions of 100 mm (width) × 100 mm (length) × 200 mm (height). To investigate some fundamental mechanical properties, measurements including uniaxial compressive test, ultrasonic testing, and weighing were

conducted. The results indicate that the corresponding uniaxial compressive strength is 123 MPa, the *P* wave velocity of these specimens is approximately 5.3 km/s at a normal temperature, and the density is 2607 kg/m³. In addition, to facilitate observations of rock failure during the test, one surface of the specimens is divided into several subregions marked with different letters.

The object of this paper is to study the influence of initial damage on triggered rockburst. Heat-treatment to specimens was conducted to produce initial damage to the specimens. By using this method, damage can be evenly produced within a rock specimen, thereby avoiding concentrated damage or macrocracks forming in rock specimens leading to that the obtained specimen will have low strength and is unsuitable for triggered rockburst simulation. This method has been used in many other studies that involve investigations of temperature or damage on mechanical properties of a rock mass (Chen et al. 2017b; Liu and Xu 2015; Nasser et al. 2007; Peng et al. 2016b; Yang et al. 2017; Yin et al. 2012; Zhao et al. 2018; Zuo et al. 2017). The heating process can be described as follows. Twenty-one specimens are first divided into 7 groups. Then, these specimens are heated to a temperature of 25 (without heating), 200, 300, 400, 500, or 600 °C. Specimens heated to 700 °C will be severely damaged and are not suitable for a rockburst simulation. Consequently, specimens heated to 600 °C or less are used in the present study. In addition, to ensure uniform damage, the specimens were evenly heated with a stepwise heating method at an increasing rate of 2 °C/min, which should be sufficiently slow to avoid thermal shock. After the temperature increased to the prescribed value for an hour, the heated specimens were spontaneously cooled to room temperature. Rapid thermal cooling, which can also significantly damage the rock specimen by inducing considerable fractures, should be avoided.

To examine the effect of thermal treatment on the microstructure of the specimen, a scanning microscope (SEM) was used to reveal the microscopic features of the rock specimens treated with various temperatures. The SEM images of the rock specimen with an amplification factor of 2000 for different initial damage conditions are presented in Fig. 2. It can be seen that as the temperature increases, the flatness of the surface of the tested specimen decreases. When the temperature is below 300 °C, the surface of the tested specimen is still flat and no newly formed fractures can be observed. For temperatures above 300 °C, the surfaces are out-of-plane and thermally induced microcracks are obvious. This description is similar to the results obtained with optical measurements for westerly granite (Nasser et al. 2007; Yin et al. 2012).

For convenience, the *P* wave velocity is always used to evaluate the damage of rocks (Liu and Xu 2015; You et al. 2008; Zhang et al. 2011) even though only a statistical relation, instead of a mechanical relation, exists between the *P* wave velocity and the strength and elastic modulus of rocks

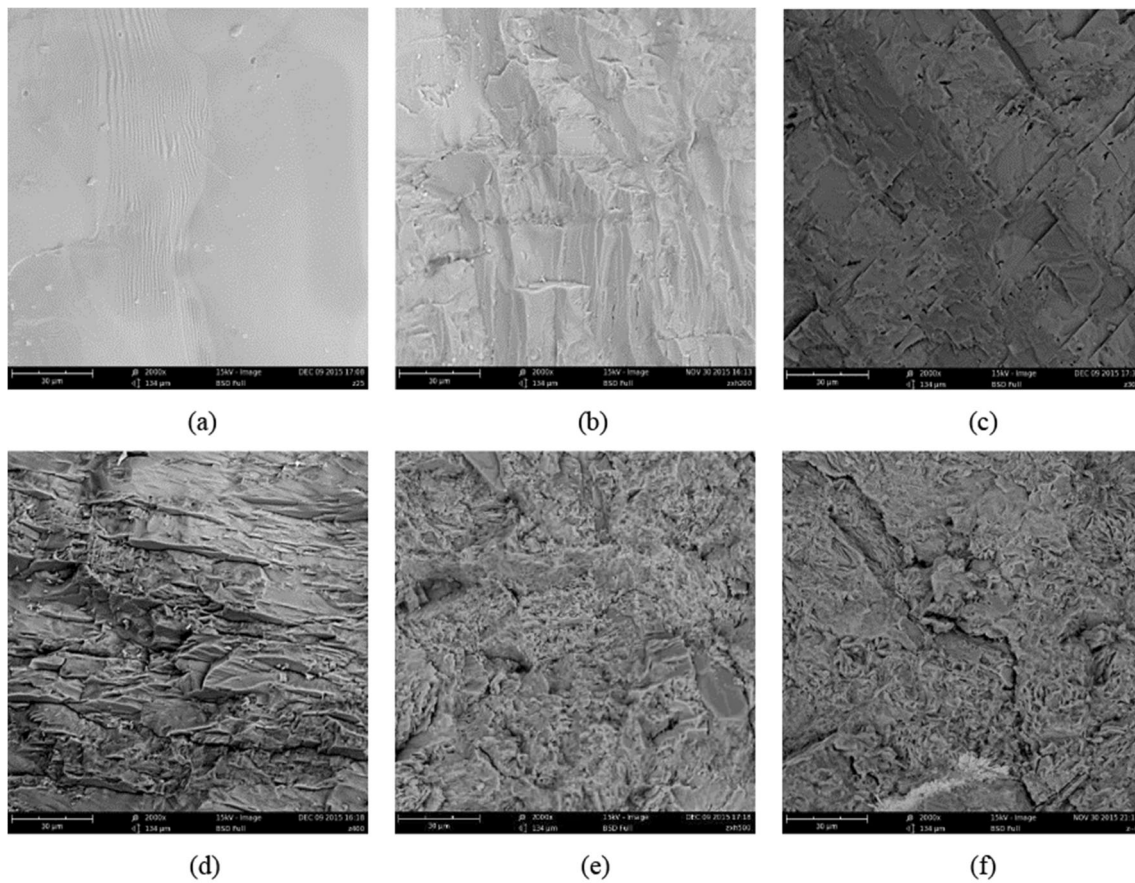


Fig. 2 SEM photos of the sections of the specimen with different initial damages. **a** $D=0$ without heat-treated, **b** $D=0.2$ with a heat-treated temperature of 200 °C, **c** $D=0.3$ with a heat-treated temperature of 300 °C, **d**

$D=0.4$ with a heat-treated temperature of 400 °C, **e** $D=0.6$ with a heat-treated temperature of 500 °C, **f** $D=0.7$ with a heat-treated temperature of 600 °C

(Jin et al. 2018). In the present study, first the ultrasonic P wave velocity of the tested specimens is measured using a supersonic reflectoscope and listed in Table 1. Then, the initial damage D of the heat-treated specimens can be calculated using the following formula (Liu and Xu 2015):

$$D = 1 - \frac{v^2}{v_0^2} \quad (1)$$

where v is the longitudinal wave velocity of the specimens after heat-treatment, and v_0 is the longitudinal wave velocity of the tested specimens without heat-treatment. The initial damages of the specimens treated with different temperatures are listed in Table 1. For the specimen without heat-treatment, D is assumed to be 0. As the heating temperature increases, the initial damage D increases, which is consistent with the SEM observation.

Testing equipment

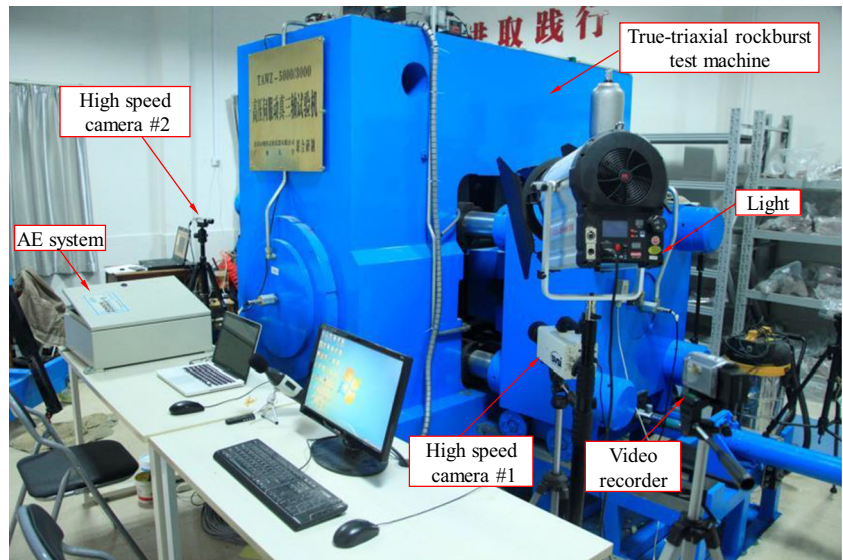
The object of the present study is to investigate remotely triggered rockburst. An apparatus for applying coupled static-

dynamic loading is needed. As shown in Fig. 3, a rigid true-triaxial rockburst testing machine is used. It can load or unload along three mutually independent directions with an output force of 5000 kN along the vertical direction and 3000 kN along the horizontal direction. In addition, this machine can also apply a dynamic disturbance on a tested specimen along the vertical direction and a horizontal direction with a disturbance rod, as shown in Fig. 4. A dynamic disturbance with a maximum amplitude of 500 kN and maximum frequency of

Table 1 Initial damage of the specimens heat-treated at different temperatures

Temperature T (°C)	Velocity of longitudinal wave v (km/s)	Initial damage D
25	5.2	0
200	4.7	0.18
300	4.4	0.28
400	4.0	0.41
500	3.3	0.60
600	2.8	0.71

Fig. 3 Testing equipment



50 Hz can be achieved. The dynamic disturbance can be in the shape of a sine, triangular, or square waveform. Furthermore, a linear variable differential transducer (LVDT), a high-speed camera system, a digital camera, and an acoustic emission (AE) system were utilized to monitor the rock failure during the testing process.

Loading path

The deformation behavior and failure of rock mass is closely related to the stress and boundary condition. Hence, when investigating a triggered rockburst, the stress state and boundary condition of the related rocks before the triggered rockburst should be determined. As shown in Fig. 5, a stress concentration always occurs in the rocks after excavation, i.e., the tangential stress σ_θ (corresponding to the maximum principal stress σ_1) of the rock mass near an excavated boundary continually rises, which leads to an accumulation of elastic

strain energy. Before the tangential stress increases to its peak value, the stressed rocks are vulnerable to a dynamic disturbance $P(t)$. When encountering an external dynamic disturbance (Fig. 6) caused by blasting and drilling, an adjacent rockburst, or seismic activity, a dynamic rock failure accompanied by ejection of rock fragments may occur. This type of rock failure is generally called triggered rockburst. A triggered rockburst can be produced in the laboratory if the loading path is reasonably represented.

In previous literature, the rock masses near the excavated boundary are supposed to be in a uniaxial or biaxial stress state. The failure of these rock masses is usually investigated by conducting uniaxial or biaxial tests. In those situations, the radial stresses are ignored. However, under a highly stressed ground condition, the radial stresses of the rock masses near the excavated boundary exhibit a gradient variation with the increases of the distance away from the excavated boundary. On the excavated boundary, the radial stress vanishes, while

Fig. 4 Schematic drawing of the dynamic loading device. **a** Disturbance device, **b** Tested specimen under dynamic and static loading

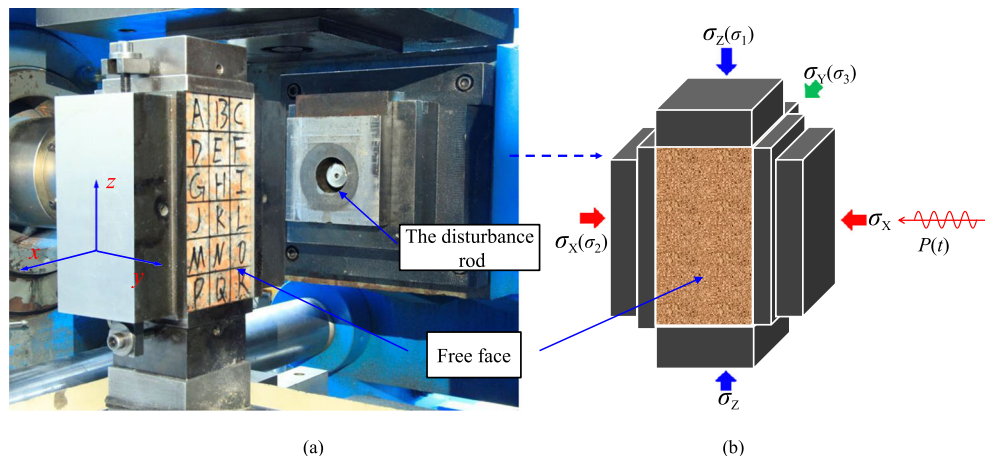
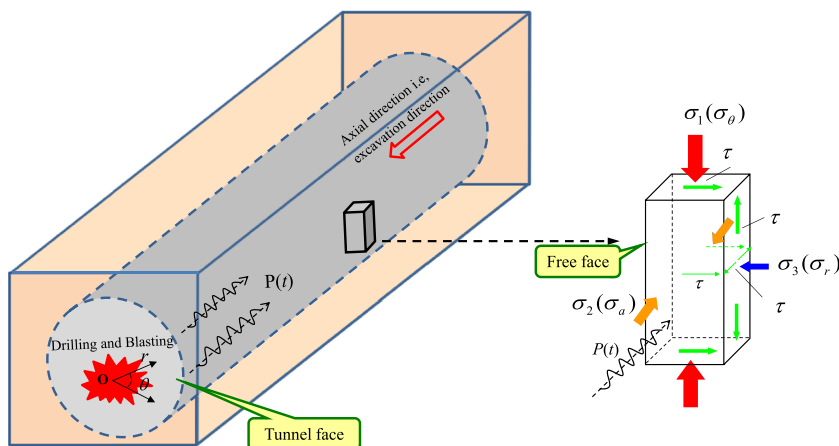


Fig. 5 Stress state of a typical rock element near the free boundary after excavation (Su et al. 2017b)



the radial stresses swiftly grow as the distance of the rock element from the excavated boundary increases. This radial stress gradient will result in a different rock mechanical response based on the influence of the confining pressure on the rock failure, as shown in previous literature (Brady and Brown 2013; Haimson and Chang 2000; Mogi 2007). It is therefore necessary to consider the radial stress gradient when studying a rockburst. This variation can be simulated by applied asymmetric stresses, i.e., keeping one-free face and loading on the other free faces on a specimen with a relatively larger thickness. Therefore, as described in “Specimen Preparation” section, the specimens used in the present study have a thickness of 100 mm.

In the present study, a loading path presented in Fig. 7 is used to simulate the stress change of the rock mass during the triggered rockburst process (Su et al. 2017b). This loading path can be described in detail as follows. First, to simulate the static stress state of a rock mass after excavation, asymmetric stresses were applied on a rectangular prismatic rock specimen, i.e., one face remained stress free and the stresses on the other faces were simultaneously increased to the predetermined values with a loading rate of 0.5 MPa/s. Then, a sinusoidal disturbance $P(t)$ with a frequency of 20 Hz and an amplitude of 100 kN was applied on the stressed specimen along the X direction to mimic the stressed rock mass near the excavation subject to a low-frequency dynamic disturbance. The prescribed duration of the dynamic disturbance was 5 min.

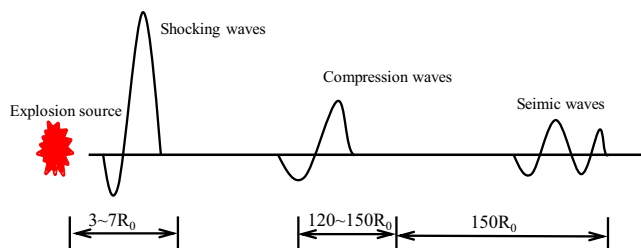


Fig. 6 Map of the evolution of an explosion stress wave in rocks (Li et al. 2009)

In addition, it should be pointed out that after trial and error, we found that when σ_z is higher than 230 MPa, all the tested specimens will fail in a self-initiated rockburst manner during increasing the quasi-static stress. Meanwhile, when σ_z is lower than 180 MPa, the tested specimens will not exhibit rockburst manner. The object of our study is triggered rockburst. Consequently, the maximum and minimum of σ_z are 230 MPa and 180 MPa, respectively. To obtain a better understanding of the influence of σ_z on triggered, σ_z between 230 MPa and 180 MPa, i.e., 200 MPa is also chosen.

Results and discussion

Influence of initial damage on the failure mode

Three failure modes including triggered rockburst, self-initiated rockburst, and slabbing are involved in the present study, as shown in Table 2.

It can be seen that for a specific predetermined maximum Z-direction static stress (σ_z), the failure of the tested specimen under different initial damage condition varies. When the predetermined maximum Z-direction static stress is 230 MPa,

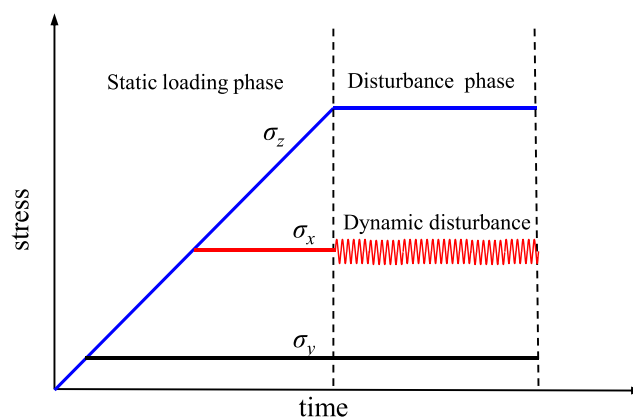


Fig. 7 Loading path

Table 2 Failure mode of the tested specimen under different loading conditions

Specimen no.	D	Predetermined σ_{zmax}/MPa	Actual σ_{zmax}/MPa	σ_x/MPa	σ_y/MPa	Amplitude A/MPa	Frequency f/Hz	Failure mode
T-1	0	230	230	30	5	5	20	Triggered rockburst
T-2	0.2	230	230	30	5	5	20	Triggered rockburst
T-3	0.3	230	230	30	5	5	20	Triggered rockburst
T-4	0.4	230	210	30	5	–	–	Self-initiated rockburst
T-5	0.6	230	191	30	5	–	–	Self-initiated rockburst
T-6	0.7	230	185	30	5	–	–	Self-initiated rockburst
T-7	0	200	200	30	5	5	20	None fracture
T-8	0.2	200	200	30	5	5	20	None fracture
T-9	0.3	200	200	30	5	5	20	Slabbing
T-10	0.4	200	200	30	5	5	20	Triggered rockburst
T-11	0.6	200	189	30	5	–	–	Self-initiated rockburst
T-12	0.7	200	186	30	5	–	–	Self-initiated rockburst
T-13	0	180	180	30	5	5	20	None fracture
T-14	0.2	180	180	30	5	5	20	None fracture
T-15	0.3	180	180	30	5	5	20	None fracture
T-16	0.4	180	180	30	5	5	20	Slabbing
T-17	0.6	180	180	30	5	5	20	Triggered rockburst
T-18	0.7	180	180	30	5	5	20	Triggered rockburst

for the tested specimen (T-1, T-2, and T-3) with initial damages of 0, 0.2, and 0.3, respectively, the failure model is a triggered rockburst, i.e., a dynamic failure induced by a disturbance during the dynamic loading stage. For the tested specimens (T-4, T-5, and T-6) with initial damages of 0.4, 0.6, and 0.7, respectively, a dynamic rock failure was encountered in the static loading stage, which is referred to as self-initiated rockburst. When σ_z is 200 MPa, the tested specimens (T-7 and T-8) with initial damages of 0 and 0.2, respectively, show no obvious failure; the tested specimen (T-9) with an initial damage of 0.3 shows a slabbing failure; the failure mode of the tested specimens (T-10 and T-11) with initial damages of 0.4 and 0.6, respectively, is a triggered rockburst, and the tested specimen (T-12) with an initial damage of 0.7 shows a self-initiated rockburst manner. When σ_z is 180 MPa, the tested specimens (T-13, T-14, and T-15) with initial damages of 0, 0.2, and 0.3, respectively, show no obvious failure; the tested specimen (T-16) with an initial damage of 0.4 shows a slabbing failure, and the failure mode of the tested specimens (T-17 and T-18) with initial damages of 0.6 and 0.7, respectively, is a triggered rockburst. Therefore, the initial damage significantly influences the failure mode of the tested specimens.

In addition, the initial damage also affects the strength of the tested specimen under the one-free-face true-triaxial compression condition. Using the tested specimen with a

predetermined maximum Z-direction static stress of 230 MPa as an example, the corresponding actual σ_z of tested specimens (T-1, T-2, and T-3) is 230 MPa, which equals the predetermined maximum Z-direction static stress. While, σ_z of the tested specimens (T-4, T-5, and T-6) with initial damages of 0.4, 0.6, and 0.7 are 210, 190, and 185 MPa, respectively, which are significantly lower than the predetermined Z-direction static stress of 230 MPa. The result indicates that damage reduces the strength of the rocks, and there is an initial damage threshold beyond which the rock strength significantly decreases. This finding matches well with the conclusions in the previous publications (Chen et al. 2017a; Su et al. 2017a). A conclusion of this paper is that an increase in initial damage decreases the needed static stress to induce rock failure. In other words, a rockburst can be much more easily triggered under high initial damage conditions, and the initial damage will increase the likelihood of a rockburst. This finding is consistent with the investigative results of 335 rockburst cases encountered during the construction of the Jinping II Hydropower Station (Feng et al. 2013). Most of these rockbursts appeared in less intact rock masses, as shown in Fig. 8, irrespective of the percentage of triggered rockbursts of these 335 rockbursts.

For a given initial damage, the failure mode of the tested specimens with different predetermined maximum Z-

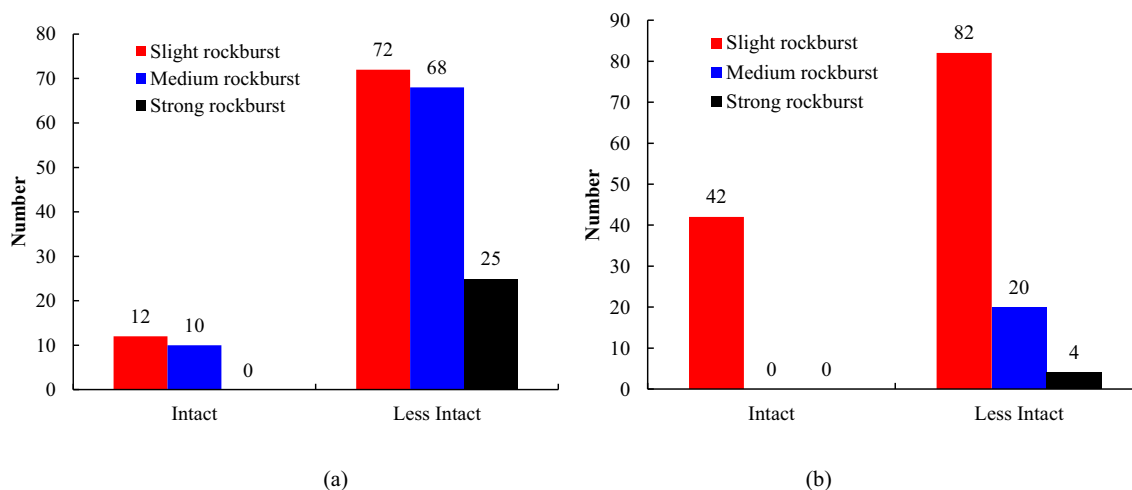


Fig. 8 Numbers of rockbursts that occurred during the construction of the Jinping II Hydropower Station during excavation using **a** drilling and blasting and **b** TBM (Feng et al. 2013)

direction static stresses varies. Under low initial damage conditions, for example, the specimens (T-2, T-8, and T-14) with an initial damage of 0.2, in which the predetermined maximum Z-direction static stress is 230 MPa, the failure mode of the tested specimen is a triggered rockburst; when the predetermined maximum Z-direction static stress is 200 MPa or 180 MPa, the tested specimens show no obvious dynamic failure. It can be concluded that for a given initial damage, a threshold of static stress exists beyond which a dynamic disturbance can induce a triggered rockburst. Otherwise, stressed rock masses fail statically or even show no failure. Under high initial damage conditions, for example the specimens (T-5, T-11, and T-17) with initial damage of 0.6, in which the predetermined maximum Z-direction static stresses are 230 and 200 MPa, the failure mode of the tested specimens is a self-initiated rockburst and the actual maximum Z-direction stresses are all 190 MPa; when the predetermined maximum Z-direction static stress is 180 MPa, a triggered rockburst occurred. Therefore, we can infer that the increased initial damage lowers the static stress threshold. A self-initiated rockburst will occur if the rock masses are not subjected to a dynamic disturbance before the tangential stress increases to its maximum. Consequently, the static stress also significantly influences the failure mode of the rocks.

It should be noted that the critical concern in the present work is the triggered rockburst. Therefore, the obtained testing data of specimens T-1, T-2, T-3, T-10, T-17, and T-18 are investigated.

Influence of initial damage on the stress-strain behavior

Figure 9 shows the Z-direction stress-strain curves of the tested specimens (T-1, T-2, T-3, T-10, T-17, and T-18) with different initial damages of 0, 0.2, 0.3, 0.4, 0.6, and 0.7,

respectively. It indicates that the tested specimens experience similar mechanical behaviors during the static loading period, dynamic loading period, and rapidly declining stress period. (1) In the first period, the stress nonlinearly increases (corresponding to rock compaction) followed by a linear rise (corresponding to rock elastically deforming) as the strain increases, which leads to high elastic strain energy stored in the rock specimen. These energies are the source that drives the final rock failure, i.e., a triggered rockburst. There is no unstable crack development, and the rock specimens still have integrity and a high carrying capacity. (2) In the second period, the dynamic disturbance continually degrades the rock specimen, which corresponds to the relatively flat section of the stress-strain curve characterized by a continual increasing strain with a constant stress. This behavior is similar to plastic flow after rock yielding. The carrying capacity and energy storage limit of the rock specimen decrease gradually. (3) Finally, the carrying capacity decreases to a constant static stress, and the energies are instantly released in the form of a triggered rockburst. The stress dramatically drops once the overall failure occurs. From the above description, we can see that the dynamic disturbance is the inducing factor for a triggered rockburst.

Initial damage affects the mechanical behavior of the tested specimens, and significant differences in the rock mechanical behavior for different initial damage conditions can be obtained, as shown in Fig. 9. The rock specimen with a high initial damage experiences long microcracks compaction, which is consistent with the results of ultrasonic and SEM testing. After the microcracks compact, the rock specimen deforms elastically. Specifically, the corresponding elastic modulus (i.e., the slope of the straight-line segment of the stress-strain curve before applying a dynamic disturbance) under the initial damages of 0, 0.2, 0.3, 0.4, 0.6, and 0.7 is 34.67, 34.55, 33.52, 25.67, 26.35, and 22.44 GPa, respectively. Obviously, the

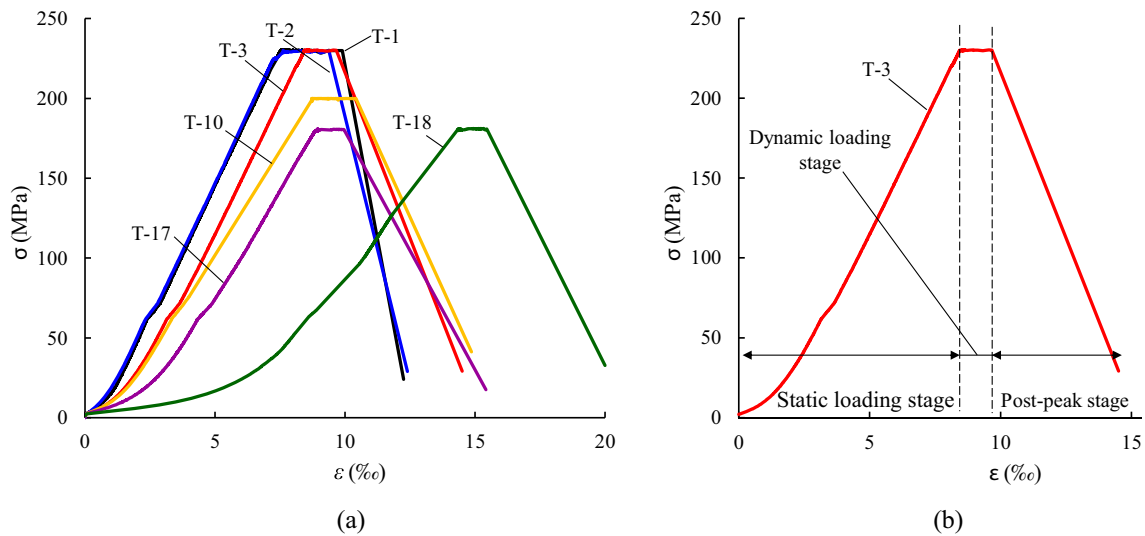


Fig. 9 Stress-strain behavior. **a** Z-direction stress-strain curves of tested specimens for different initial damage conditions, the initial damage D of specimens T-1, T-2, T-3, T-10, T-17, and T-18 are 0, 0.2, 0.3, 0.4, 0.6, and 0.7, respectively; **b** Three typical stages that the tested specimens experienced (specimen T-3 is the example)

elastic modulus decreases as the initial damage (heat-treatment temperature) increases. This relationship agrees with the results obtained in other studies (Chen et al. 2012; Liu and Xu 2014; Liu and Xu 2015; Yang et al. 2017), which demonstrates the validity and reasonability of the experimental data to some extent. Additionally, the increased initial damage reduces the elastic modulus of the tested specimen. Additionally, as the initial damage increases, the Z-direction strain during static loading significantly increases. These strains are 7.47‰, 7.38‰, 8.38‰, 8.77‰, 9.22‰, and 14.49‰ under the initial damages of 0, 0.2, 0.3, 0.4, 0.6, and 0.7, respectively.

By using the elastic modulus E and stress σ_z , the elastic strain energy U_e accumulated in the tested specimens before applying a dynamic disturbance under different initial damages can be calculated using the following formula

$$U_e = V \frac{\sigma^2}{2E} \tag{2}$$

where V is the volume of a specimen. In the present study, V is 0.002 m^3 ($0.1 \text{ m} \times 0.1 \text{ m} \times 0.2 \text{ m}$). As shown in Table 3, the rocks with a lower initial damage sustain a larger external force, which causes higher stress within the rocks. Higher stress always corresponds to more elastic strain energy before rock failure (He et al. 2015; Su et al. 2017c). Hence, the elastic strain energies of tested specimens T-1, T-2, and T-3 with low initial damages of 0, 0.2, and 0.3 are much greater than those of tested specimen T-10, T-17, and T-18 with high initial damages of 0.4, 0.6, and 0.7. Furthermore, the elastic strain energy is a controlling factor that induces a rockburst. Hence, tested specimens with a low initial damage generally show a more

violent failure behavior than those with a high initial damage.

Furthermore, it can be found from Table 3 that under the same static Z-direction stress, the elastic strain energy of a tested specimen with a lower initial damage is relatively higher. For example, when the static Z-direction stress is 230 MPa, the elastic strain energy of tested specimens T-1, T-2, and T-3 increases as the corresponding initial damage increases (0, 0.2, and 0.3, respectively). Two reasons may be involved. The first is that the low elastic modulus favors the accumulation of elastic strain energy according to Eq. (1). This is the reason why considerable efforts have been devoted to increasing the stiffness of the testing machine in the past few decades. A testing machine with low rigidity (elastic modulus) will store abundant elastic strain energy during the loading process. These energies will be released when the rock failure occurs and thereby increase the intensity of the rock failure. In this situation, the actual energy evolution of the rocks during the failure process is concealed; therefore, the energy results are unreasonable and prevent discovery of the rock failure mechanism. The second reason is that the elastic modulus that corresponds to the high initial damage is low, as described above. Otherwise, from Table 3, it is clear that although the static Z-direction stress (200 MPa) of tested specimen T-10 is obviously lower than the 230 MPa of tested specimen T-1, the elastic strain energy of specimen T-10 is similar to specimen T-1. This is attributed to the hypothesis that the elastic modulus of tested specimen T-10 is much lower than that of tested specimen T-1. Consequently, a different conclusion from those in the previous studies can be drawn. Higher rock strength does not always correspond to larger accumulated elastic strain energy within a rock mass when the initial damage or elastic modulus is involved.

Table 3 Elastic strain energy U_e accumulated in tested specimens before applying a dynamic disturbance

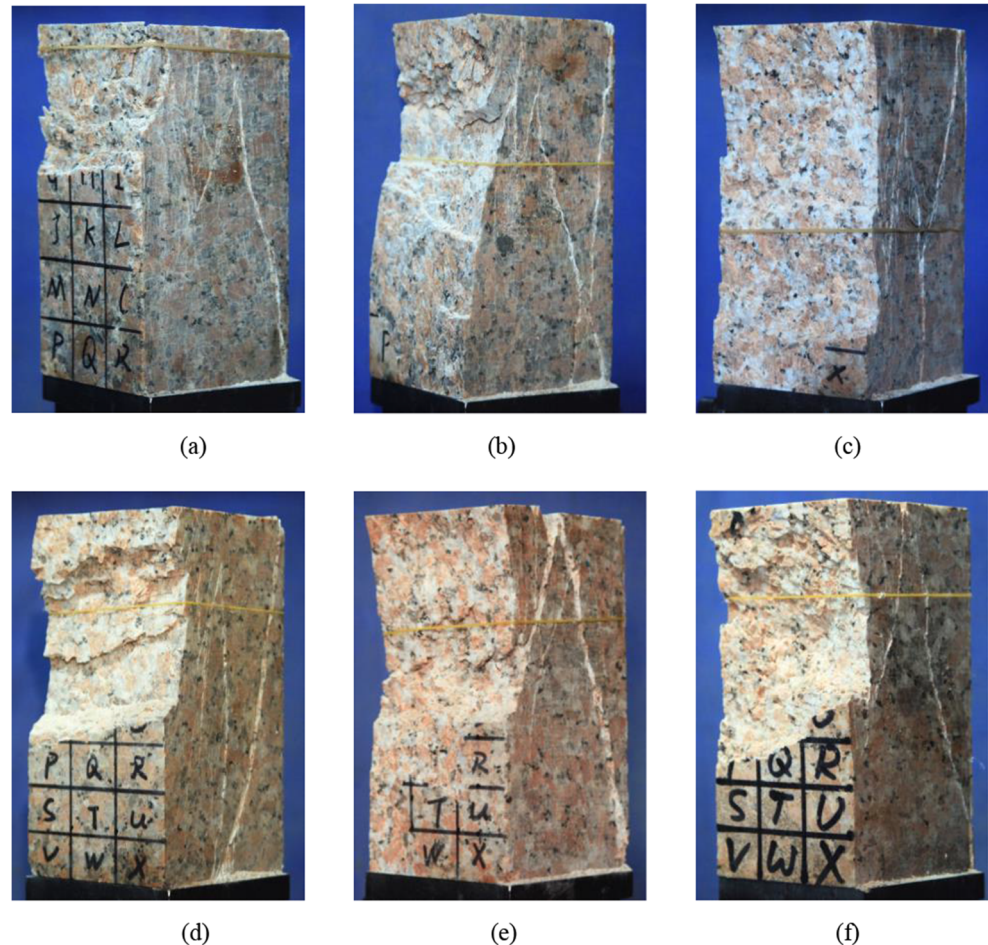
Specimen no.	Initial damage	Elasticity modulus (GPa)	Static Z-direction stress σ_z (MPa)	Elastic strain energy U_e (J)
T-1	0	34.67	230	3051.6
T-2	0.2	34.55	230	3062.2
T-3	0.3	33.52	230	3156.3
T-10	0.4	25.67	200	3116.5
T-17	0.6	26.35	180	2459.2
T-18	0.7	22.44	180	2887.7

Influence of initial damage on rock fracture

Figure 10 indicates that all the tested specimens show a similar zoning failure form, i.e., V-shaped or stepwise rockburst pits near the free face and macro shear fractures away from the free face. This zoning failure form is caused by the gradient stress along σ_y , which has been described in detail in the literature (Su et al. 2017c). The area of the rockburst pits under different initial damage conditions apparently varies. When the initial damage is 0.2 or 0.3, the rockburst pit covers almost all of the

free face of the tested specimen. While under other initial damage conditions, the rockburst only destroys part of the free face. Consequently, as the initial damage increased, the area of the rockburst pit increased and then decreased; the tested specimen with an initial damage of 0.3 had a relatively larger rockburst pit region. A larger rockburst pit area does not mean a greater rockburst scale. The depth of the rockburst pit should be taken into consideration to determine the rockburst scale. The depth of the rockburst pits under different initial damage conditions is shown in Fig. 11. As the initial damage D

Fig. 10 Failure forms of the tested specimens for different initial damage conditions. **a** $D=0$, **b** $D=0.2$, **c** $D=0.3$, **d** $D=0.4$, **e** $D=0.6$, **f** $D=0.7$



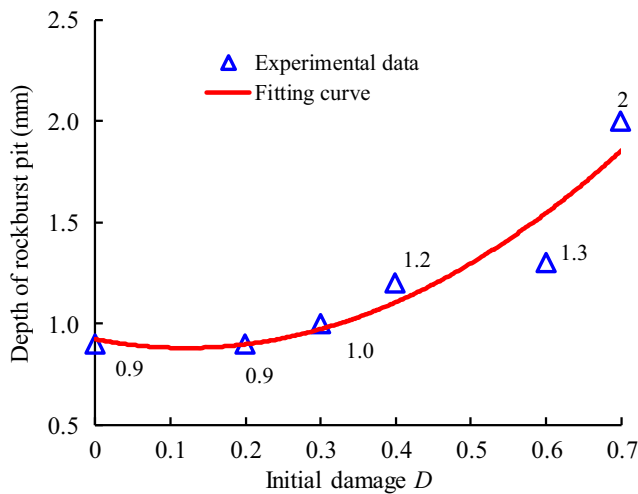


Fig. 11 Curve of initial damage D versus depth of rockburst pit

increases, the depth increases. Then, the equivalent volume of the rockburst pits can be calculated, as shown in Table 4. It can be seen that the volume of the rockburst pits of the tested specimen increased as the initial damage increased. The tested specimen with an initial damage of 0.7 had the largest rockburst pit volume, and therefore, the corresponding rockburst scale was the largest. However, the rockburst intensity remains unascertainable and should be investigated in terms of the dissipated energy and kinetic energy during a rockburst. The dissipated energy can be analyzed according to the following fragments characteristic investigation, while the kinetic energy of the ejected fragments will be discussed in detail in “Influence of initial damage on remotely triggered rockburst intensity” section.

Average size is a significant characteristic of fragments. Consequently, the average size of the fragments of the tested specimen for different initial damage conditions was determined using a statistical approach. This method is described in the details that follow. First, all the fragments collected after rockburst are divided into several groups using sieves (Li et al. 2010; Su et al. 2017a; Wang et al. 2019). In this study, the fragments are classified into 9 groups of fragment sizes, $d <$

0.075 mm , $0.075 < d < 0.15 \text{ mm}$, $0.15 < d < 0.3 \text{ mm}$, $0.3 < d < 0.6 \text{ mm}$, $0.6 < d < 1.18 \text{ mm}$, $1.18 < d < 2.36 \text{ mm}$, $2.36 < d < 4.75 \text{ mm}$, $4.75 < d < 9.5 \text{ mm}$, and $d > 9.5 \text{ mm}$ (Fig. 12). The mass of the rock fragments m_i ($i = 1, 2, 3, 4, 5, 6, 7, 8,$ and 9) in each group was measured. Then, the average size of the fragment \bar{d} is calculated by

$$\bar{d} = \sum_{i=1}^9 w_i \hat{d}_i \tag{3}$$

where, w_i denotes the right, and \hat{d}_i is the equivalent size.

$$w_i = \frac{m_i}{\sum m_i} \tag{4}$$

$$\hat{d}_i = \begin{cases} \frac{d_i}{2} & i = 1 \\ \frac{d_{i-1} + d_i}{2} & 1 < i < 9 \\ \frac{\sum l_{\max}}{n} & i = 9 \end{cases} \tag{5}$$

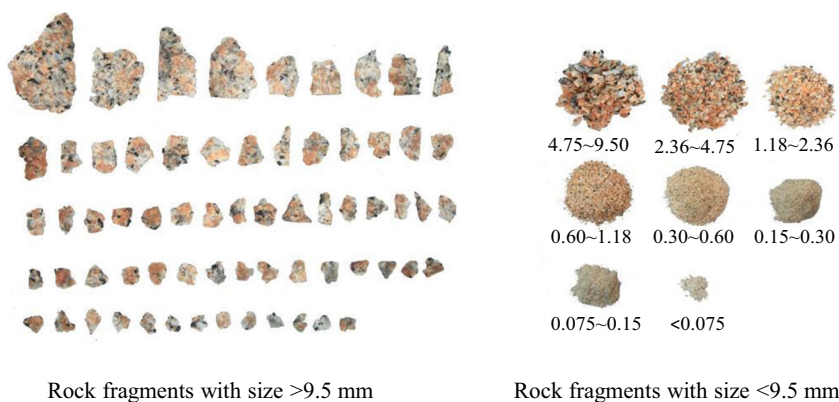
where d_i is the sieve pore of the sieving instrument listed in Table 5, l_{\max} is the maximum length of fragments with a size larger than 9.5 mm, and n is the number of fragments for a given size.

Figure 13 presents the average size of fragments of the tested specimen for different initial damage conditions. The fragments of the tested specimen with an initial damage of 0.3 have an maximum average size. A slight increasing trend for the average size was obtained for initial damage up to 0.3. After initial damage of 0.3, as the damaged increases, the average size decreases rapidly. The average size of the fragments can indicate the damage degree of the tested specimen and the corresponding dissipated energy during the rockburst process. The smaller the size of the fragments, the more energy is needed to form them and the more seriously the tested specimen is damaged (Li et al. 2010; Liu et al. 2014; Wang et al. 2019). Hence, the minimum dissipated energy of the tested specimens occurred with an initial damage of 0.3, which may contribute to this condition causing the most

Table 4 Size of the rockburst pits of the tested specimens for different initial damage conditions

Specimen no.	Initial damage	Rockburst pit			
		Length L (cm)	Width W (cm)	Depth D (cm)	Volume ($LWD/3$) (cm ³)
T-1	0	0.84	1.0	0.9	0.25
T-2	0.2	1.82	1.0	0.9	0.55
T-3	0.3	1.86	1.0	1.0	0.62
T-10	0.4	1.71	1.0	1.2	0.68
T-17	0.6	1.69	1.0	1.3	0.73
T-18	0.7	1.64	1.0	2.0	1.09

Fig. 12 Fragments of the tested specimen for the initial damage $D = 0$ condition



intense rockburst. The dissipated energy of the tested specimen with initial damage of 0.7 is the largest. As the initial damage increases, the dissipated energy increases and then decreases.

The characteristic of the fragments can partially represent the rock failure mechanism. The typical coarse and medium fragments of the tested specimen for the initial damages of 0, 0.3, and 0.7 are shown in Fig. 14. The fragments with a maximum size beyond 9.5 mm are defined as coarse fragments, while the ones with a maximum size between 4.75 mm and 9.5 mm are defined as medium fragments in the present study. For the coarse fragments, the width-to-thickness ratio of the tested specimens with initial damages of 0, 0.3, and 0.7 are 7.2, 5.2, and 2.5, respectively. For the medium fragments, the width-to-thickness ratio of the tested specimens with initial damages of 0, 0.3, and 0.7 are 2.9, 1.67, and 1.2, respectively. Apparently, as the initial damage increases, the width-to-thickness ratio significantly decreases and the shape of coarse fragments changes from lamellar to blocky.

Influence of initial damage on remotely triggered rockburst intensity

Remotely triggered rockbursts under different initial damages have a similar development process, as shown in Fig. 15. During the static loading period, no apparent rock failure occurs. Then, the specimens are subjected to a dynamic disturbance. In the early stage of the dynamic disturbance period, the tested specimen still shows no failure. As the dynamic disturbance continues, small rock fragments accompanied by ringing cracking sounds can be observed. During the late stage of the dynamic disturbance period, rock elements near the free

face split and form rock plates. Subsequently, the rock plates expand with continuous ringing sounds. When the expansion is significant enough, the rock plates break, and the broken plates and fragments are abruptly ejected out accompanied by a huge sound. In summary, the rockburst process includes ejection of particles, rock elements splitting into rock plates, bending of the rock plate, and ejection of rock fragments as soon as the rock plates break. This process is consistent with that in other triggered rockburst studies (Su et al. 2017b; Su et al. 2018).

Figure 16 presents the duration T_b of the dynamic disturbance with the same frequency and amplitude for different initial damage D conditions for specimens subjected to a remotely triggered rockburst. As D increases, T_b decreases. The duration of the dynamic disturbance T for a high initial damage condition is significantly less than that for a low initial damage condition. For example, T_b for the tested specimen with an initial damage of 0.2 is 120.6 s, while T_b for the tested specimen with an initial damage of 0.6 is 36 s. This difference indicates that the dynamic disturbance can much more easily trigger a rockburst for the high initial damage condition. As

Table 5 d_i of the rock fragments in each ground (unit:mm)

d_1	d_2	d_3	d_4	d_5	d_6	d_7	d_8
0.075	0.15	0.30	0.60	1.18	2.36	4.75	9.5

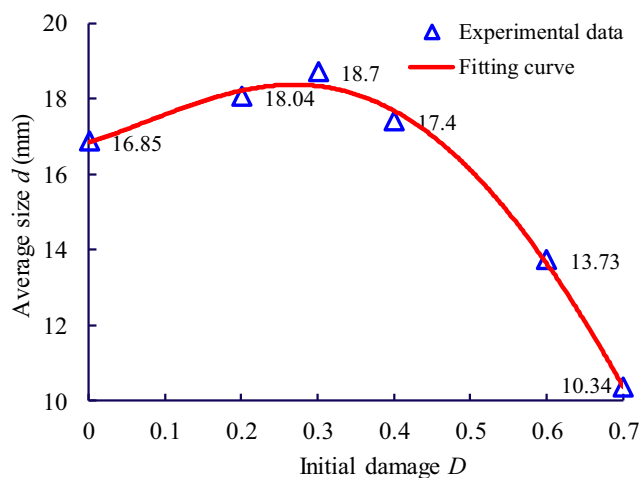
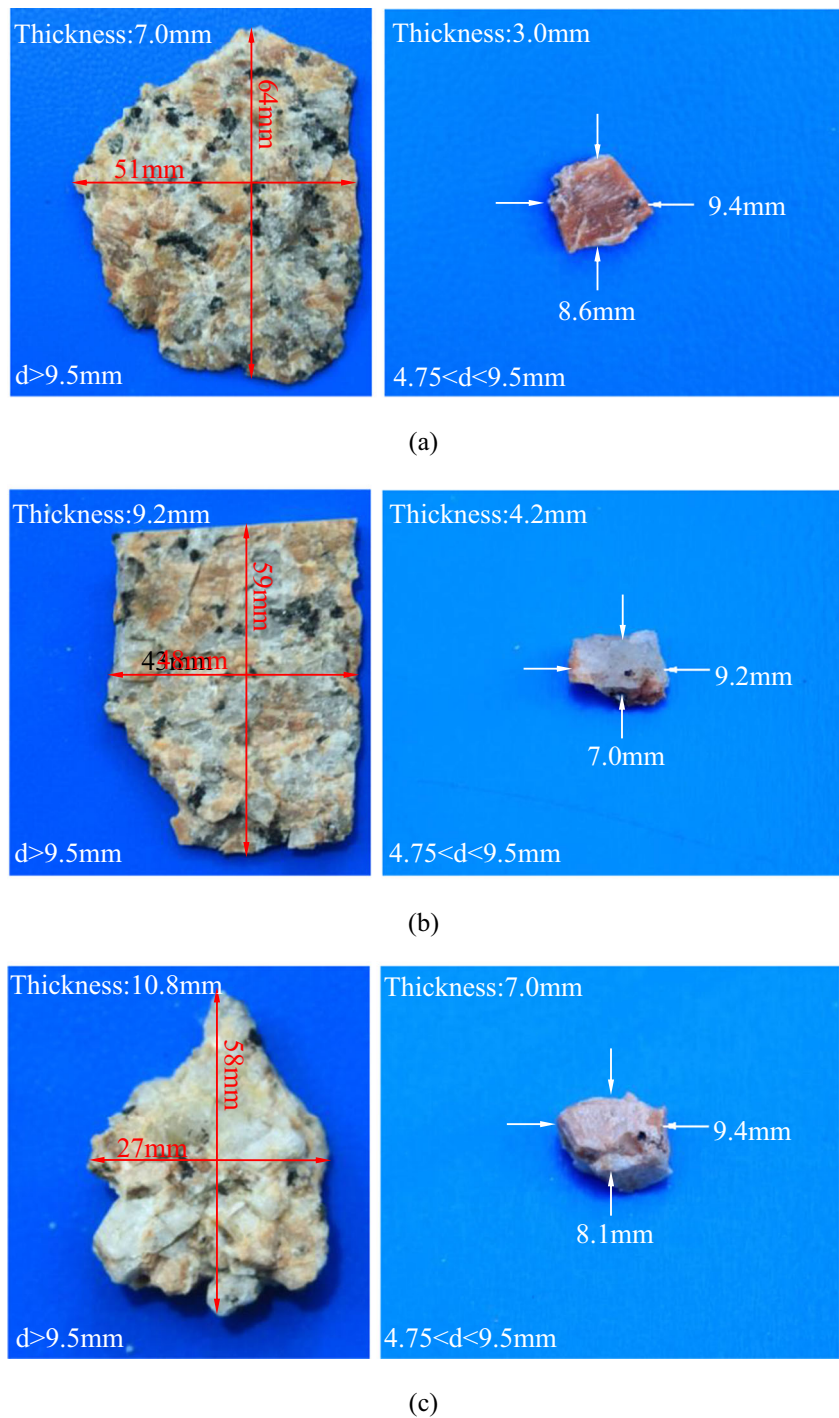


Fig. 13 Average size of the fragments of the tested specimen for different initial damages D

Fig. 14 Coarse fragments of the tested specimens with initial damages of **a** 0, **b** 0.3, and **c** 0.7

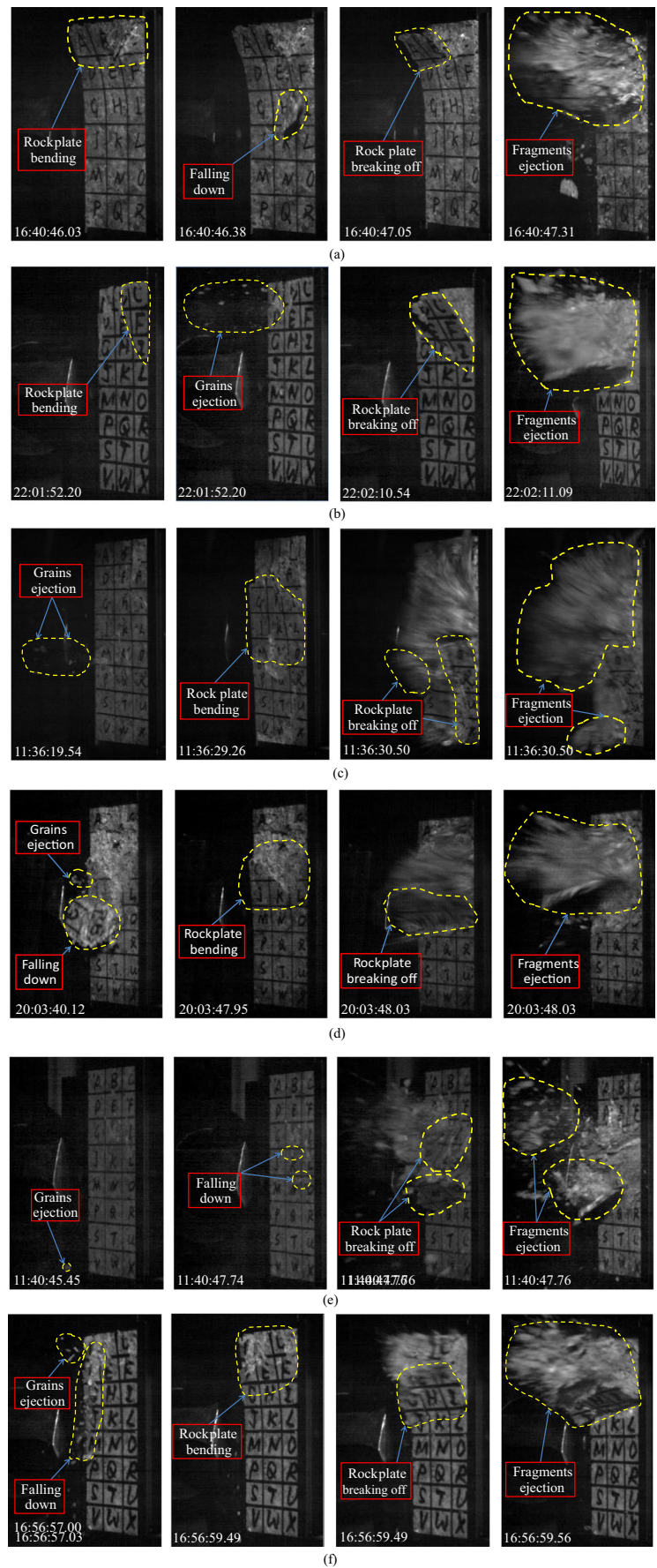


the initial damage increases, the likelihood of a remotely triggered rockburst increases. It should be pointed out that the intensity of the rockburst is different with the likelihood. The intensity will be systematically investigated according to the kinetic energy of the ejected fragments during rockburst process.

During underground excavation, the primary threat of a rockburst to workers and construction equipment is ejected

fragments. Therefore, the kinetic energy of the ejected fragments can be used to quantitatively evaluate the intensity of a rockburst. In the present study, the kinetic energy is obtained by measuring the speed and mass of the ejected fragments. A high-precision scale can directly measure the mass. To obtain the speed of the ejected fragments, an image analysis software, Image Pro Plus 7.0 depicted in Fig. 17, was utilized to analyze the recorded video of the

Fig. 15 Rockburst process of the tested specimen for different initial damage conditions. **a** $D = 0$, **b** $D = 0.2$, **c** $D = 0.3$, **d** $D = 0.4$, **e** $D = 0.6$, **f** $D = 0.7$



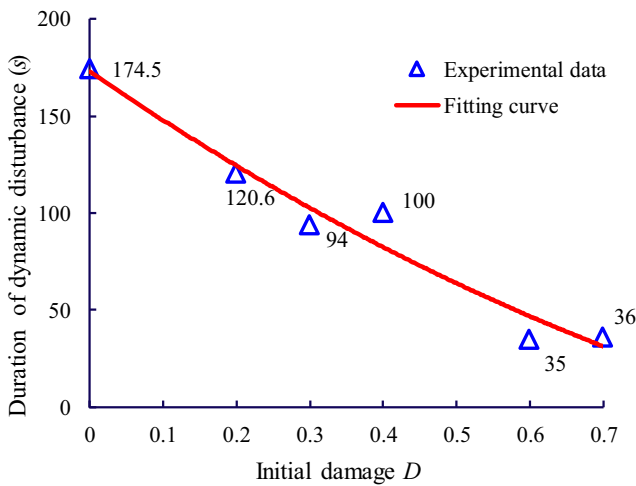


Fig. 16 Curve of the initial damage versus duration of the dynamic disturbance

rock failure process. First, the trajectories of the ejected fragments were automatically or manually captured. Then, the speed of ejected fragments was calculated by dividing the distance along the trajectory by the corresponding time interval.

As shown in Fig. 18, the failure process of the tested specimen during the testing process was primarily recorded by high-speed camera #1 with a recording rate of 500 frames per second (fps). The video recorded by high-speed camera #2 supplements the first video. It should be noted that there are angles between the recording direction of the high-speed cameras and the ejection path of the rock fragments. For high-speed camera #1, the angle is 60°. For high-speed camera #2, the angle is 75°. Hence, a transform should be implemented to change the measured speed to the actual speed (Su et al. 2017c).

The detailed process of calculating the kinetic energy is described as follows:

- Step 1: For the fragments with a size greater than 9.50 mm, the speed of four feature points and the centroid point are measured; then, the average of the speed of these points is recorded.
- Step 2: For the fragments with a size between 4.75 mm and 9.50 mm, the speed of several fragments is calculated, and the average of the speed of the fragments is recorded.
- Step 3: For the fragments with a size less than 4.75 mm, the speed of the fragments in different locations is calculated, and the average of the speed of the fragments is recorded.
- Step 4: The kinetic energy of the ejected fragments with different sizes can be calculated according to Eq. (5). Then, the total kinetic energy of the ejected fragments can be obtained.

$$E_k = \frac{1}{2}mv^2 \tag{6}$$

Figure 19 shows the kinetic energy of the tested specimens for different initial damage conditions. The kinetic energy of the ejected fragments for low initial damages (0, 0.2, 0.3, and 0.4) is generally higher than those for high initial damages (0.6 and 0.7), indicating a higher intensity of triggered rockburst under lower initial damage conditions. For example, the kinetic energy of the ejected fragment for the initial damage of 0.2 is 5.75 J, which is significantly larger than 1.93 J for the initial damage of 0.7. Furthermore, another interesting finding is the nonlinear relation of the kinetic energy of the ejected fragments with initial damage. The kinetic energy, i.e., intensity of the triggered rockburst, first increases and then decreases as the initial damage increases. The most suitable initial damage of the tested specimens is 0.3. For this initial damage, the kinetic energy is a maximum, i.e., the corresponding triggered rockburst is the most intense. This can be explained as follows.

Fig. 17 Example of measuring the speed of the ejected fragments using Image PropPlus 7.0

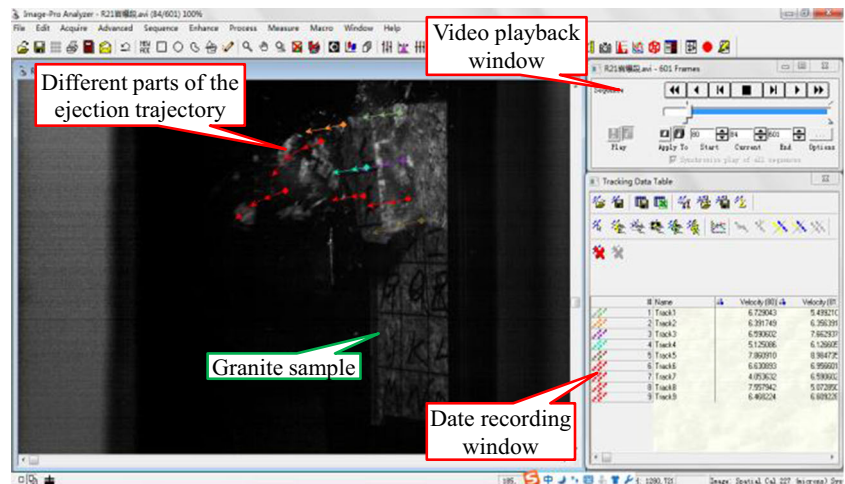
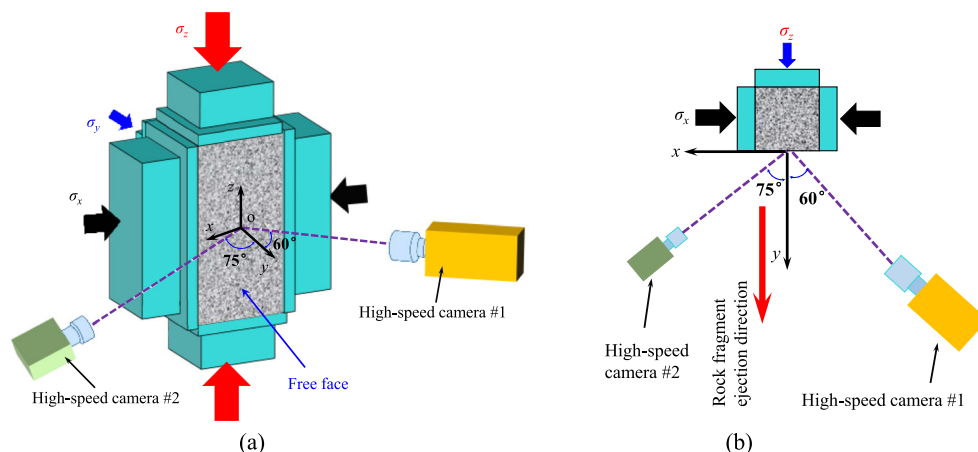


Fig. 18 Layout of the high-speed cameras. **a** Stereogram, **b** Planform



From the viewpoint of energy, during the triggered rockburst process, the kinetic energy of the ejected fragments is proportional to the difference between the accumulated elastic strain energy before applying a dynamic disturbance and the dissipated energy during rock failure, which can be described as follows:

$$E_k = \alpha(U_e - U_d) \tag{7}$$

where U_e is the accumulated elastic strain energy; U_d is the dissipated energy during rock failure; the difference between these energies is called the residual energy; and α is the ratio of translating the residual energy into kinetic energy. Hence, both a higher U_e and lower U_d can produce a larger kinetic energy. The variation of the kinetic energy as the initial damage increases can be explained in terms of the accumulated strain energy and dissipated energy during rock failure. Coincidentally, the maximum U_e and minimum U_d occur when the initial damage is 0.3 in the present study.

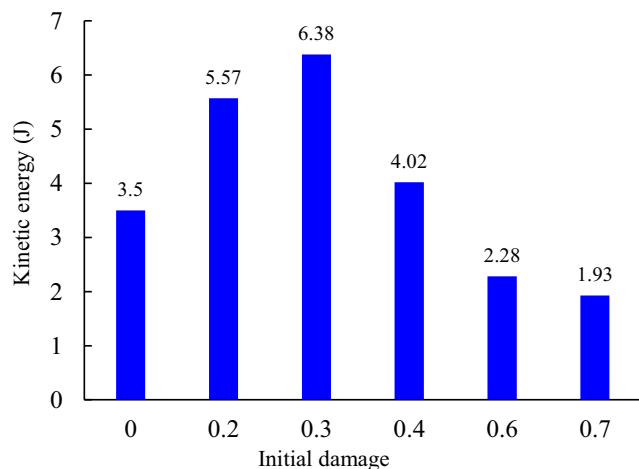


Fig. 19 Kinetic energy of the tested specimens for different initial damage conditions

Therefore, the corresponding kinetic energy is the highest for this condition, which will be discussed in the details that follow.

As initial damage increases from 0 to 0.3, the elastic modulus of the tested specimen decreases. Meanwhile, the tested specimens sustain the same maximum stress of 230 MPa. Therefore, the elastic strain energy accumulated before applying a dynamic disturbance for an initial damage of 0.3 is the maximum value. On the other hand, the existing microcracks significantly affect the fracture process of the rock mass. New microcracks generally generate along existing microcracks, which in turn promote the propagation and coalescence of existing microcracks that eventually induce the overall rock failure. The initial damages of 0.2 and 0.3 are produced using the heat-treatment method with temperatures of 200 °C and 300 °C, respectively. As shown in Fig. 2, no obvious new microcracks can be observed when the temperature is below 300 °C. However, as the temperature increases, the initial damage of the tested specimen does increase. This can be attributed to the fact that the length of the microcracks instead of the number of the existing microcrack increases. The length of the microcracks of the tested specimen with initial damage of 0.3 is the largest. During an overall failure, the longer microcracks can coalesce much more easily and dissipate less energy compared with those for initial damages of 0 and 0.2. This is consistent with the fact that the average size of the fragment for an initial damage of 0.3 is smaller than that for the initial damage of 0 and 0.2. Meanwhile, the post-peak dissipated energy is mainly caused by the fracture process. Therefore, the kinetic energy for an initial damage of 0.3 is higher than that for initial damages of 0 and 0.2. As the initial damage increases from 0 to 0.3, the increment of the kinetic energy is (2.88 J) 82.3%.

As the initial damage increases from 0.3 to 0.7, the elastic modulus of the tested specimens decreases. However, the corresponding static stress for the tested specimen with initial damage of 0.3 is much higher than those with initial damages

of 0.4, 0.6, and 0.7. Consequently, the elastic strain energy for an initial damage of 0.3 is the maximum value. Meanwhile, as shown in Fig. 2, newly formed thermal microcracks (new microcracks induced by heat-treatment) can be found on the surfaces of the tested specimen for initial damages of 0.4, 0.6, and 0.7, i.e., both the number and length of the microcracks increase during heat-treatment. Due to the increased length, the existing microcracks can propagate and coalesce much more easily, thereby dissipating less energy than those with an initial damage greater than 0.3 during testing. However, the evolution of the newly formed thermal microcracks will dissipate more energy. The total dissipated energy caused by the evolution of the existing and newly formed thermal microcracks for initial damage greater than 0.3 is higher than that the dissipated energy only caused by the evolution of existing microcracks for initial damage greater than 0.3. In addition, this total dissipated energy increases as the initial damage increases. Consequently, the kinetic energy for the initial damage of 0.3 is higher than the kinetic energies for initial damages of 0.4, 0.6, and 0.7. As the initial damage increases, the kinetic energy decreases with an amplitude of (4.55 J) 69.7%.

The discussion above focuses on the pattern of increasing and then decreasing kinetic energy as the initial damage increases and provides a reason why the largest kinetic energy occurs for an initial damage of 0.3. Further review of the kinetic energy shows that the kinetic energy when the initial damage is 0.4 approaches the kinetic energy when the initial damage is 0.

When the initial damage is 0.4, the static stress is lower than when the initial damage is 0. However, the corresponding elastic modulus when the initial damage is 0.4 is also lower. Hence, the elastic strain energy for an initial damage of 0.4 is similar to that when the initial damage is 0, as shown in Table 3. In addition, newly formed thermal microcracks are introduced by heat-treatment into the tested specimen with an initial damage of 0.4, but the number of newly formed microcracks is small. The total dissipated energy caused by the evolution of the newly formed and existing microcracks for the initial damage condition is still less than that only caused by the evolution of the existing microcrack for an initial damage of 0. This is verified by the fact that the average size for the initial damage = 0 is smaller than that for the initial damage = 0.4. Therefore, the kinetic energy for an initial damage of 0.4 is slightly higher than that for an initial damage of 0.

For an initial damage of 0.6, the sustained static stress (180 MPa) is relatively low; the length of the existing microcracks significantly increases and many thermal microcracks form during heat-treatment. The accumulated elastic strain energy of the tested specimen with an initial damage of 0.6 is lower than the tested specimen with an initial damage of 0, as shown in Table 3, and the corresponding postpeak dissipated energy is higher. Consequently, the

kinetic energy for an initial damage of 0.6 is approximately 35% lower than that for an initial damage of 0.

Furthermore, the static stresses under the initial damages of 0.6 and 0.7 are 180 MPa. Simultaneously, the elastic modulus for an initial damage of 0.6 is higher than that for an initial damage of 0.7. Consequently, the accumulated elastic strain energy for an initial damage of 0.6 is smaller. However, the corresponding kinetic energy is higher, because many more microcracks are formed in the specimen with an initial damage of 0.7 during heat-treatment at 600 °C. Most of the accumulated elastic strain energy will be dissipated by the propagation and coalescence of the microcracks during testing process. Hence, the kinetic energy for an initial damage of 0.7 is extremely low.

The aforementioned experimental results provide knowledge about the influence of initial damage on remotely triggered rockbursts for engineering practice.

For a tunnel excavated using the drilling and blasting method (transient release of in situ stress), the surrounding rock mass will be seriously damaged, which leads to an increased likelihood of remotely triggered rockbursts, i.e., a remotely triggered rockburst can be induced much more easily. Corresponding support measurements should be implemented to lower the risk of a triggered rockburst. For a tunnel excavated using the TBM method (quasi-static unloading of in situ stress) only slightly damages the rock masses; the likelihood of a remotely triggered rockburst is relatively low. However, once a remotely triggered rockburst occurs, the corresponding intensity will be high especially under a high geo-stress condition, because that more intact rock mass can accumulate more elastic strain energy. Engineering measures such a stress relief aperture should be applied to decrease the intensity of a potential remotely triggered rockburst. However, it should be noted that the damage degree should be sufficiently increased. In the present study, the kinetic energy will significantly decrease only when the initial damage is greater than 0.6. Otherwise, both the likelihood and intensity of the remotely triggered rockburst will increase.

Conclusions

The present paper investigates the influence of the initial damage on a triggered rockburst. Granite specimens with different initial damages ($D = 0, 0.2, 0.3, 0.4, 0.6, \text{ and } 0.7$) were tested under the true-triaxial condition. During a test, the specimen was subjected to coupled static and dynamic loading. The failure mode, deformation characteristics, fracture features, and kinetic energy of the ejected fragments of the tested specimen were systematically investigated. The following conclusions are drawn:

- (1) For a given initial damage and dynamic disturbance, a threshold of static stress exists, beyond which a triggered rockburst can be induced by a dynamic disturbance. Otherwise, the stressed rock masses slab or show no failure. In contrast, a self-initiated rockburst will occur if the rock masses are not subjected to a dynamic disturbance before the major principal stress increases to a high value. In addition, a triggered rockburst can be much more easily induced by a dynamic disturbance as the initial damage increases. For a high initial damage condition, the required static stress is low, and the duration of the dynamic loading is short.
- (2) As the initial damage increases, the elastic modulus decreases. The elastic strain energies for low initial damage (0, 0.2, and 0.3) conditions are larger than those for high initial (0.4, 0.6, and 0.7) damage conditions. In addition, higher rock strength does not always correspond to larger accumulated elastic strain energy within the rock mass when initial damage and elastic modulus are involved.
- (3) As the initial damage increases, the area of the rockburst pit increases and then decreases, the depth of the rockburst pits increases, the corresponding volume of the rockburst pit increases, and the average size of the fragments decreases, which indicates an increasing energy dissipation; furthermore, the width-depth ratio of the fragments shows a decreasing trend, and the shape of the fragment changes from sheet to blocky.
- (4) The initial damage of the tested specimen significantly affects the kinetic energy of the ejected fragments during a rockburst. The kinetic energy of the ejected fragments of a triggered rockburst increases and then decreases as the initial damage increases, and the maximum kinetic energy appears at an initial damage $D = 0.3$, which indicates that this is suitable initial damage of granite that can induce the most intensive triggered rockburst. The maximum kinetic energy for an initial damage of 0.3 is approximately 60% higher than that for an initial damage of 0. Furthermore, the kinetic energy of the ejected fragment for an initial damage less than 0.6 is larger than that for an initial damage of 0. The kinetic energy will be lower than that for an initial damage of 0 only when the initial damage is greater than 0.6.

Note that the present study was an indoor investigation of small-sized rock specimens. The stress state or boundary of the rocks simulated using testing machine in laboratory, to some extent, may differ from that in situ. For example, the applied dynamic disturbance is a simplification of a field dynamic disturbance wave caused by blasting and drilling. Thus, it is necessary to conduct in situ rockburst tests. Moreover, remotely triggered rockbursts also occur in supported rock masses; therefore, it is indispensable to investigate remotely triggered rockbursts in a supported condition.

Funding information This study received financial support from the National Natural Science Foundation of China (Grant Nos. 51869003, 51809051).

References

- Akdag S, Karakus M, Taheri A, Nguyen G, He MC (2018) Effects of thermal damage on strain burst mechanism for brittle rocks under true-triaxial loading conditions. *Rock Mech Rock Eng*:1–26
- Board M, Fairhurst C (1983) Rockburst control through destressing—a case example. In: *Proceedings of the conference on rockbursts*, British Institute of Mining and Metallurgy, pp 91–101
- Brady BHG, Brown ET (2013) *Rock mechanics: for underground mining*. Springer Science & Business Media
- Cai M (2013) Principles of rock support in burst-prone ground. *Tunn Undergr Space Technol* 36:46–56
- Chen GQ, Li TB, Zhang GF, Yin HY, Zhang H (2014) Temperature effect of rock burst for hard rock in deep-buried tunnel. *Nat Hazards* 72: 915–926
- Chen LQ, Zhang JS, Chen JH, Chen JG (2017a) Influences of initial damage on mechanics of brittle rock under compressed stress. *J Cent South Univ* 48:484–490
- Chen YL, Ni J, Shao W, Azzam R (2012) Experimental study on the influence of temperature on the mechanical properties of granite under uni-axial compression and fatigue loading. *Int J Rock Mech Min Sci* 56:62–66
- Chen YL, Wang SR, Ni J, Azzam R, Fernández-Steeseer TM (2017b) An experimental study of the mechanical properties of granite after high temperature exposure based on mineral characteristics. *Eng Geol* 220:234–242
- Cho SH, Ogata Y, Kaneko K (2005) A method for estimating the strength properties of a granitic rock subjected to dynamic loading. *Int J Rock Mech Min Sci* 42:561–568
- Cook NGW (1963) The basic mechanics of rockbursts. *J South Afr Inst Min Metall* 63:71–81
- Dai F, Xia KW (2010) Loading rate dependence of tensile strength anisotropy of Barre granite. *Pure Appl Geophys* 167:1419–1432
- Doan ML, D'Hour V (2012) Effect of initial damage on rock pulverization along faults. *J Struct Geol* 45:113–124
- Fakhimi A, Hosseini O, Theodore R (2016) Physical and numerical study of strain burst of mine pillars. *Comput Geotech* 74:36–44
- Fan Y, Lu WB, Zhou YH, Yan P, Leng ZD, Chen M (2016) Influence of tunneling methods on the strainburst characteristics during the excavation of deep rock masses. *Eng Geol* 201:85–95
- Feng GL, Feng XT, Chen BR, Xiao YX (2015) Microseismic sequences associated with rockbursts in the tunnels of the Jinping II hydropower station. *Int J Rock Mech Min Sci* 80:89–100
- Feng GL, Feng XT, Chen BR, Xiao YX (2017) A highly accurate method of locating microseismic events associated with rockburst development processes in tunnels. *IEEE Access* 5:27722–27731
- Feng XT, Chen BR, Zhang CQ, Li SJ, Wu SY (2013) *Mechanism, warning and dynamic control of rockburst development processes*. Science Press, Beijing (in Chinese)
- Feng XT, Yu Y, Feng GL, Xiao YX, Chen BR, Jiang Q (2016) Fractal behaviour of the microseismic energy associated with immediate rockbursts in deep, hard rock tunnels. *Tunn Undergr Space Technol* 51:98–107
- Gong FQ, Si XF, Li XB, Wang SY (2019a) Experimental investigation of strain rockburst in circular caverns under deep three-dimensional high-stress conditions. *Rock Mech Rock Eng* 52:1459–1474
- Gong FQ, Wu C, Luo S, Yan JY (2019b) Load-unload response ratio characteristics of rock materials and their application in prediction of rockburst proneness. *Bull Eng Geol Environ* 78:5445–5466

- Gong FQ, Yan JY, Li XB, Luo S (2019c) A peak-strength strain energy storage index for rock burst proneness of rock materials. *Int J Rock Mech Min Sci* 117:76–89
- Höfer KH, Thoma K (1968) Triaxial tests on salt rocks. *Int J Rock Mech Min Sci Geomech Abstr* 5:195–196
- Haimson B, Chang C (2000) A new true triaxial cell for testing mechanical properties of rock, and its use to determine rock strength and deformability of Westerly granite. *Int J Rock Mech Min Sci* 37:285–296
- He MC, Miao JL, Feng JL (2010) Rock burst process of limestone and its acoustic emission characteristics under true-triaxial unloading conditions. *Int J Rock Mech Min Sci* 47:286–298
- He MC, Miao JL, Li DJ, Wang CG (2007) Experimental study on rockburst processes of granite specimen at great depth. *Chin J Rock Mech Eng* 26:865–876
- He MC, Xia HM, Jia XN, Gong WL, Fei Z, Liang KY (2012) Studies on classification, criteria and control of rockbursts. *J Rock Mech Geotech Eng* 4:97–114
- He MC, Zhao F, Cai M, Du S (2015) A novel experimental technique to simulate pillar burst in laboratory. *Rock Mech Rock Eng* 48:1833–1848
- Hedley DGF (1992) Rockburst handbook for Ontario hardrock mines SP92-1E. Canmet, Ottawa
- Hu XC, Su GS, Chen GY, Mei SM, Feng XT, Mei GX, Huang XH (2019) Experiment on rockburst process of borehole and its acoustic emission characteristics. *Rock Mech Rock Eng* 52:783–802
- Hua AZ, You MQ (2001) Rock failure due to energy release during unloading and application to underground rock burst control. *Tunn Undergr Space Technol* 16:241–246
- Huang RQ, Wang XN (1999) Analysis of dynamic disturbance on rock burst. *Bull Eng Geol Environ* 57:281–284
- Huang RQ, Wang XN, Chan LS (2001) Triaxial unloading test of rocks and its implication for rock burst. *Bull Eng Geol Environ* 60:37–41
- Huang ZP, Tang CA, Cai M (2018) Numerical analysis of unloading-induced rock failure: insight into strainburst mechanism. *Ind Geotech J* 48:558–563
- Jiang Q, Feng XT, Xiang TB, Su GS (2010) Rockburst characteristics and numerical simulation based on a new energy index: a case study of a tunnel at 2,500 m depth. *Bull Eng Geol Environ* 69:381–388
- Jiang Q, Su GS, Feng XT, Cui J, Pan PZ, Jiang JQ (2015) Observation of rock fragment ejection in post-failure response. *Int J Rock Mech Min Sci* 74:30–37
- Jin PH, Hu YQ, Shao JX, Zhao GK, Zhu XZ, Li C (2018) Experimental study on physico-mechanical and transport properties of granite subjected to rapid cooling. *Chin J Rock Mech Eng* 37:2556–2564
- Kaiser PK (1996) Canadian rockburst support handbook: prep. for sponsors of the Canadian rockburst research. Geomechanics Research Centre.
- Kaiser PK, Cai M (2012) Design of rock support system under rockburst condition. *J Rock Mech Geotech Eng* 4:215–227
- Li XB, Ling TH, Zhang YP (2009) Analysis choose your option of blast vibration signals-theories and methods. Science Press, Beijing (in Chinese)
- Li DJ, Jia XN, Miao JL, He MC, Li DD (2010) Analysis of fractal characteristics of fragments from rockburst test of granite. *Chin J Rock Mech Eng* 29:3280–3289
- Li SJ, Feng XT, Li ZH, Chen BR, Zhang CQ, Zhou H (2012) In situ monitoring of rockburst nucleation and evolution in the deeply buried tunnels of Jinping II hydropower station. *Eng Geol* 137-138:85–96
- Li XB, Du K, Li DY (2015) True triaxial strength and failure modes of cubic rock specimens with unloading the minor principal stress. *Rock Mech Rock Eng* 48:2185–2196
- Liu DQ, Li DJ, Zhao F, Wang CC (2014) Fragmentation characteristics analysis of sandstone fragments based on impact rockburst test. *J Rock Mech Geotech Eng* 6:251–256
- Liu S, Xu JY (2014) Mechanical properties of Qinling biotite granite after high temperature treatment. *Int J Rock Mech Min Sci* 71:188–193
- Liu S, Xu JY (2015) An experimental study on the physico-mechanical properties of two post-high-temperature rocks. *Eng Geol* 185:63–70
- Manouchehrian A, Cai M (2017) Analysis of rockburst in tunnels subjected to static and dynamic loads. *Chin J Rock Mech Eng* 9:1031–1040
- Manouchehrian A, Cai M (2018) Numerical modeling of rockburst near fault zones in deep tunnels. *Tunn Undergr Space Technol* 80:164–180
- Mao R, Mao X, Zhang L, Liu R (2015) Effect of loading rates on the characteristics of thermal damage for mudstone under different temperatures. *Int J Rock Mech Min Sci* 25:797–801
- Mogi K (2007) Experimental rock mechanics. Taylor & Francis
- Nasser MHB, Schubnel A, Young RP (2007) Coupled evolutions of fracture toughness and elastic wave velocities at high crack density in thermally treated westerly granite. *Int J Rock Mech Min Sci* 44:601–616
- Nemat-Nasser S, Horii H (1982) Compression-induced nonplanar crack extension with application to splitting, exfoliation, and rockburst. *J Geophys Res Sol Ea* 87:6805–6821
- Ortlepp WD, Stacey TR (1994) Rockburst mechanisms in tunnels and shafts. *Tunn Undergr Space Technol* 9:59–65
- Peng J, Rong G, Cai M, Yao MD, Zhou CB (2016a) Comparison of mechanical properties of undamaged and thermal-damaged coarse marbles under triaxial compression. *Int J Rock Mech Min Sci* 83:135–139
- Peng J, Rong G, Cai M, Yao MD, Zhou CB (2016b) Physical and mechanical behaviors of a thermal-damaged coarse marble under uniaxial compression. *Eng Geol* 200:88–93
- Pu YY, Apel DB, Xu HW (2019) Rockburst prediction in kimberlite with unsupervised learning method and support vector classifier. *Tunn Undergr Space Technol* 90:12–18
- Qiu SL, Feng XT, Zhang CQ, Xiang TB (2014) Estimation of rockburst wall-rock velocity invoked by slab flexure sources in deep tunnels. *Can Geotech J* 51:520–539
- Simser B, Joughin W, Ortlepp W (2002) The performance of Brunswick Mine's rockburst support system during a severe seismic episode. *J S Afr Inst Min Met* 102:217–223
- Su GS, Chen ZY, Ju JW, Jiang JQ (2017a) Influence of temperature on the strainburst characteristics of granite under true triaxial loading conditions. *Eng Geol* 222:38–52
- Su GS, Feng XT, Wang JH, Jiang JQ, Hu LH (2017b) Experimental study of remotely triggered rockburst induced by a tunnel axial dynamic disturbance under true-triaxial conditions. *Rock Mech Rock Eng* 50:2207–2226
- Su GS et al (2018) True triaxial experimental study of rockbursts induced by ramp and cyclic dynamic disturbances. *Rock Mech Rock Eng* 51:1027–1045
- Su GS, Jiang JQ, Zhai SB, Zhang GL (2017c) Influence of tunnel axis stress on strainburst: an experimental study. *Rock Mech Rock Eng* 50:1551–1567
- Su GS, Zhai SB, Jiang JQ, Zhang GL, Yan LB (2017d) Influence of radial stress gradient on strainbursts: an experimental study. *Rock Mech Rock Eng* 50:2659–2676
- Sun X, Xu H, He M, Zhang F (2017) Experimental investigation of the occurrence of rockburst in a rock specimen through infrared thermography and acoustic emission. *Int J Rock Mech Min Sci* 93:250–259
- Wang JA, Park HD (2001) Comprehensive prediction of rockburst based on analysis of strain energy in rocks. *Tunn Undergr Space Technol* 16:49–57
- Wang Y, Chun Z, He M, Liu D, Lin Y, Du S (2019) Fragmentation characteristics analysis of sandstone fragments for impact rockburst under different dynamic loading frequency. *Geotech Geol Eng* 37:2715–2727. <https://doi.org/10.1007/s10706-018-00789-7>

- Wu BB, Yao W, Xia KW (2016) An experimental study of dynamic tensile failure of rocks subjected to hydrostatic confinement. *Rock Mech Rock Eng* 49:3855–3864
- Xia KW, Nasser MHB, Mohanty B, Lu F, Chen R, Luo SN (2008) Effects of microstructures on dynamic compression of Barre granite. *Int J Rock Mech Min Sci* 45:879–887
- Xu NW, Li TB, Dai F, Zhang R, Tang CA, Tang LX (2016) Microseismic monitoring of strainburst activities in deep tunnels at the Jinping II hydropower station, China. *Rock Mech Rock Eng* 49:1–20
- Yang SQ, Ranjith PG, Jing HW, Tian WL, Ju Y (2017) An experimental investigation on thermal damage and failure mechanical behavior of granite after exposure to different high temperature treatments. *Geothermics* 65:180–197
- Yin TB, Li XB, Xia KW, Huang S (2012) Effect of thermal treatment on the dynamic fracture toughness of Laurentian granite. *Rock Mech Rock Eng* 45:1087–1094
- You MQ, Su CD, Li XS (2008) Study on relation between mechanical properties and longitudinal wave velocities for damaged rock samples. *Chin J Rock Mech Eng* 27:458–567
- Zhang C, Zhou H, Qiu S, Wu W (2012) Case histories of four extremely intense rockbursts in deep tunnels. *Rock Mech Rock Eng* 45:275–288
- Zhang YB, Yu GY, Tian BZ, Liu XX, Liang P, Wang YD (2017) Experimental study of acoustic emission signal dominant-frequency characteristics of rockburst in a granite tunnel. *Rock Soil Mech* 38:1258–1266
- Zhang ZZ, Gao F, Xu XL (2011) Experimental study of temperature effect of mechanical properties of granite. *Rock Soil Mech* 32:2346–2352
- Zhao XG, Cai M (2014) Influence of specimen height-to-width ratio on the strainburst characteristics of Tianhu granite under true-triaxial unloading conditions. *Can Geotech J* 52:890–902
- Zhao XG, Wang J, Cai M, Cheng C, Ma LK (2014) Influence of unloading rate on the strainburst characteristics of Beishan granite under true-triaxial unloading conditions. *Rock Mech Rock Eng* 47:467–483
- Zhao XG et al (2018) Influence of thermal treatment on the thermal conductivity of Beishan granite. *Rock Mech Rock Eng* 51:2055–2074
- Zhou H, Meng F, Zhang C, Hu D, Yang F, Lu J (2015) Analysis of rockburst mechanisms induced by structural planes in deep tunnels. *Bull Eng Geol Environ* 74:1–17
- Zhu WC, Li ZH, Zhu L, Tang CA (2010) Numerical simulation on rockburst of underground opening triggered by dynamic disturbance. *Tunn Undergr Space Technol* 25:587–599
- Zuo JP, Wang JT, Sun YJ, Chen Y, Jiang GH, Li YH (2017) Effects of thermal treatment on fracture characteristics of granite from Beishan, a possible high-level radioactive waste disposal site in China. *Eng Fract Mech* 182:425–437